Single microwave photon switch controlled by an external electrostatic field

Qian Jiang, Qingmei Hu, Bingsuo Zou, and Yongyou Zhang*
Beijing Key Lab of Nanophotonics & Ultrafine Optoelectronic Systems and School of Physics, Beijing Institute of Technology, Beijing 100081, China

(Received 3 March 2018; published 15 August 2018)

We design a single microwave photon switch through a one-dimensional waveguide coupled with a side Jaynes-Cummings system, namely, a single-mode cavity with an embedded Rydberg atom ^{87}Rb. Since the energy spectra of the ^{87}Rb atom depend on the electrostatic field, the ^{87}Rb atom can couple with the cavity in tune and out of tune, corresponding to the switch on and off states, respectively. The influences of the single photon pulse width, cavity dissipation, and Rabi coupling on the on/off ratio are studied in detail by a non-Hermitian Hamiltonian. We find that the on/off ratio can be larger than 100 in a wide parameter space and the decay time and rise time are both about 0.75 ns. Within the master equation of the density matrix we also demonstrate that the on/off ratio can be reduced by the quantum noise but is still large enough for application. The transition energy of the two-level Rydberg atom ^{87}Rb gives the switch operating frequency which is in the range of microwave regime. Accordingly, the switch is viable in practice and has potential in quantum informatics.

DOI: 10.1103/PhysRevA.98.023830

I. INTRODUCTION

Coupled architecture of one-dimensional (1D) waveguides with quantum emitters has been proposed in recent years for manipulating few-photon states due to its simple physical structure. Diverse quantum emitters include quantum dots [1–3], optomechanical cavities [4], single or multiple atoms possessing two or more levels [5–11], cavities with an atom [12,13] or a Kerr medium inside [14], and so on. The 1D waveguides can be made of line defects in photonic crystals [15–18] or micro- or nanowires [19–21]. Such coupled architecture benefits from advanced micro- and nanofabrication techniques, rousing an upsurge of study on waveguide quantum electrodynamics, for example, electromagnetically induced transparency [22–25], Fano resonance [26–28], polarization effects [29], slow light behavior [23,30], multiphoton transmission [4,14,31–33], and so on. These results inspired many attempts on designing quantum devices of photons, such as optical switches [29,34,35], single-photon transistors [36], photon memory [23], and band filters [37,38]. As a core element in informatics, optical switches could be achieved by mechanical methods [39], electro- and magneto-optic effects [40,41], or introducing nonlinear materials [42,43]. Those optical switches without moving elements are more suitable for integrating with electronic circuits.

In this work, we propose a scheme for designing a single microwave photon switch. Microwave photons were widely investigated in the context of cavity quantum electrodynamics with Rydberg atoms or superconducting circuits [45]. Several ways have been proposed for generating the single microwave photons, for example, controllable superconducting circuit architectures [46,47] and two-level systems [48]. Microwave technologies are of high interest because of their promising applications in quantum informatics, sensing, imaging, and other fields. As an example, we consider a single microwave photon with frequency of 27 GHz. The single microwave photon switch is based on the coupled architecture of a centimeter-width 1D waveguide with a Jaynes-Cummings (JC) model, as shown in Fig. 1(a). The JC model contains a quantum cavity with an embedded two-level atom in it. One typical two-level atom is the Rydberg atom, such as ^{87}Rb. Lots of work has been done for the resonator-Rydberg atom system which shows abundant fundamental physics in quantum optics and circuit quantum electrodynamics [44,49]. A merit of the Rydberg atoms is that the energy levels of their Rydberg states can be controlled effectively by an external electrostatic field, which offers a way for adjusting the eigenfrequency of quantum emitters. One of the most effective methods for achieving the photon switches is just to shift the resonant frequency of quantum emitters either toward or away from the frequency of incident signals. They include changing the refraction index of photonic crystals [50,51], using nonlinear cavities [14], and introducing an atom into quantum emitters or not [29,52]. We consider another method, namely, changing the Rydberg levels of the ^{87}Rb atom in the JC model by an external electrostatic field [see Fig. 1(a)]. It is similar to the last mentioned method but without moving the atom. The energy spectra of the Rydberg states of ^{87}Rb can be adjusted by an external electrostatic field which is controlled by U. The variation of the two concerned energy levels with the external electrostatic field is given in Fig. 1(b) (refer to Ref. [44] for more details). The ^{87}Rb atomic-qubit transition between these two levels can be tuned in or out of resonance with the cavity by the external electrostatic field [53,54] and the transition in the range of $[\omega_1,\ \omega_2] = [2.7\omega_0,\ 0.7\omega_0]$, with $\omega_0 = 2\pi \times 10^{10}$ Hz considered in the present work [see Fig. 1(b)]. As a ratiocination, the levels of the JC model can also be tuned in or out of resonance with the incident photon, which

*Author to whom correspondence should be addressed: yyzhang@bit.edu.cn

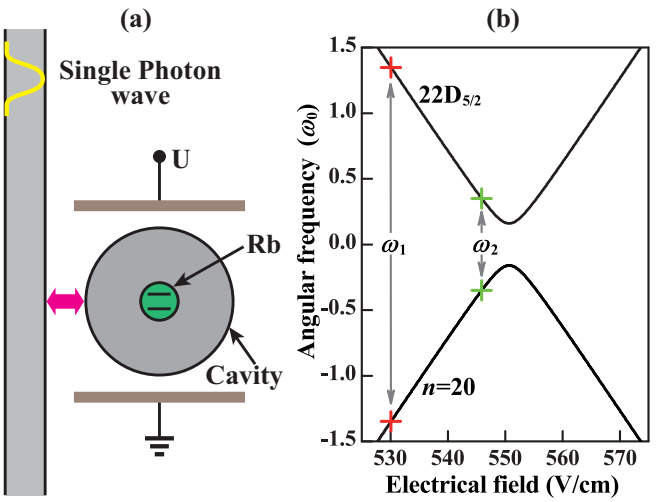

FIG. 1. (a) Schematic diagram of a one-dimensional waveguide side coupled with a cavity with eigenfrequency of ω_c. The yellow wave curve stands for a single photon pulse in the waveguide whose coupling with the cavity is denoted by the pink arrow. In the cavity a ^{87}Rb atom is embedded and the energies of its Rydberg states can be tuned by an external voltage difference of U. (b) Concerned energy spectra for ^{87}Rb in the electrostatic field (due to the direct current Stark shifts of Rydberg states), refer to Ref. [44] for details. In calculation we focus on the transition frequency range of $[\omega_1,\ \omega_2] = [2.7\omega_0,\ 0.7\omega_0]$ with $\omega_0 = 2\pi \times 10^{10}$ Hz, where ω_1 and ω_2 correspond to an electrostatic field of 530 and 545.9 V/cm, respectively.

provides a convenient way for designing a single microwave photon switch. We will study how to achieve such a single microwave photon switch and related influences of the model parameters on its performance.

The work is organized as follows. In Sec. II, the model and related Hamiltonian are introduced, including the system time-dependent dynamical equations. In Sec. III, we first examine the factors that influence the on/off ratio of the single photon pulse, including the coupling strength between the cavity and 1D waveguide, dissipations of the cavity and atom, and Rabi coupling between the cavity and atom. Then, two dynamical cases, namely, the switch is (a) turned on and then off and (b) turned off and then on, are considered to confirm the switch mechanism and to determine the switch decay time and rise time. At last, a Lindblad master equation is introduced to discuss the influence of the quantum noise on the on/off ratio. In Sec. IV, a conclusion is summarized.

II. MODEL AND FORMULAS

A. Jaynes-Cummings model

The structure of the single microwave photon switch is depicted in Fig. 1(a), where the quantum emitter is the single-mode cavity with an embedded two-level ^{87}Rb atom. When the switch works the ^{87}Rb atom is highly excited into the Rydberg states whose energy levels are controlled by an external electrostatic field of E. In the experiment, the electrostatic field is generated by an extra parallel-plate capacitor with an imposed voltage difference of U. Using the results in Ref. [44] we show the variation of the two Rydberg states in Fig. 1(b). The lowest atomic transition frequency is $\Omega = 0.32\omega_0$, with the frequency unit of $\omega_0 = 2\pi \times 10^{10}$ Hz occurring at $E = 550.7$ V/cm. When the transition frequency is near Ω, the Hamiltonian for the ^{87}Rb atom under the electrostatic field is reduced as [44]

$$\mathcal{H}_a = \frac{\tilde{\omega}_a}{2}(\hat{\sigma}_z + \hat{I}) + \frac{\Omega}{2}\hat{\sigma}_x, \tag{1}$$

where the Planck constant has been set to $\hbar = 1$ for easy writing. $\tilde{\omega}_a = \omega_a - i\gamma_a$ with the transition energy of ω_a and loss of γ_a depends on the external electrostatic field of E. $\hat{I}$ is the 2×2 unit matrix, introduced for setting the energy of the lower level to zero. $\hat{\sigma}_z$ and $\hat{\sigma}_x$ are the z and x components of the Pauli matrices, respectively. With the raising and lowering operators of $\hat{\sigma}_\pm$, they can be expressed into $\hat{\sigma}_z = \hat{\sigma}_+\hat{\sigma}_- - \hat{\sigma}_-\hat{\sigma}_+$ and $\hat{\sigma}_x = \hat{\sigma}_+ + \hat{\sigma}_-$. The expression of $\hat{\sigma}_x$ shows that the second term in Eq. (1) does not obey the conservation law of particle number. It suggests us to focus on the transition frequency that is away from the anticrossing point (minimal-gap position), for example, the range of $[\omega_1,\ \omega_2] = [2.7\omega_0,\ 0.7\omega_0]$ in Fig. 1(b), in which the second term in Eq. (1) can be neglected.

Within this approximation the Hamiltonian for the JC model of the ^{87}Rb atom coupled with one cavity reads

$$\mathcal{H}_{\rm JC} = \frac{\tilde{\omega}_a}{2}(\hat{\sigma}_z + \hat{I}) + \tilde{\omega}_c\hat{c}^\dagger\hat{c} + \frac{g}{2}(\hat{c}^\dagger\hat{\sigma}_- + \hat{\sigma}_+\hat{c}), \tag{2}$$

where $\hat{c}^\dagger$ ($\hat{c}$) is the creation (annihilation) operator of the cavity mode. The frequency $\tilde{\omega}_c = \omega_c - i\gamma_c$ with the energy of ω_c and loss of γ_c. g describes the Rabi coupling between the atom and cavity. We choose $\omega_c = \omega_1$ throughout the work. The transition frequency of the ^{87}Rb atom continuously changes from ω_1 to ω_2 as the electrostatic field increases from 530 to 545.9 V/cm. Accordingly, the atom and cavity are in resonance when $E = 530$ V/cm and are out of resonance when $E = 545.9$ V/cm. The cavity size is comparable to the wavelength of the single microwave photon ($\sim$2 cm). When the two capacitor poles are outside the cavity [see Fig. 1(a)], the voltage difference of U is $\sim$1.1 kV, while when the capacitor is in the cavity, U is mainly determined by the distance between its two poles. For the latter case, U can be very small, for example, U is $\sim$0.55 V as the distance between the two capacitor poles is $\sim$10 μm. These parameters are practical for designing the single microwave photon switch.

B. Hamiltonian and dynamical equations

When the JC model is coupled with the 1D waveguide, the full Hamiltonian can be written as

$$\begin{aligned}\mathcal{H} = &\int dx\{\hat{\psi}_R^\dagger(x)\hat{\omega}(-i\partial_x)\hat{\psi}_R(x) + \hat{\psi}_L^\dagger(x)\hat{\omega}(+i\partial_x)\hat{\psi}_L(x)\} \\ &+ \int dx\, V_0\delta(x)\{[\hat{\psi}_R^\dagger(x) \\ &+ \hat{\psi}_L^\dagger(x)]\hat{c} + \text{H.c.}\} + \mathcal{H}_{\rm JC},\end{aligned} \tag{3}$$

where $\hat{\psi}_L^\dagger(x)$ and $\hat{\psi}_L(x)$ [$\hat{\psi}_R^\dagger(x)$ and $\hat{\psi}_R(x)$] are the field operators of the left-moving (right-moving) waveguide mode, respectively. They create and annihilate a left-moving (right-moving) photon in the position eigenstate $|x\rangle$. $\hat{\omega}(\mp i\partial_x)$ is the photon kinetic energy operators, determined by the waveguide dispersion $\omega(k)$. Commonly, the waveguide dispersion

is linearized around the energy levels of the JC model for simplicity. Since the incident wave is a pulse in practice and contains many plane-wave components, it is better to use a more general waveguide dispersion for $\hat{\omega}(\mp i\partial_x)$. We take $\omega(k) = c\sqrt{k_z^2 + k^2}$ with the vacuum light speed of c, representing the dispersion of a two-dimensional confined waveguide, such as a one-dimensional rectangular waveguide or a cylindrical waveguide. k and k_z are the longitudinal and transversal wave vectors, respectively. The coupling between the waveguide and cavity is described by a δ function with strength V_0. For a general case the coupling is an overlap integral of the cavity and waveguide modes and shows a strong dependence on the distance between the cavity and waveguide [55]. The microwave cavity and waveguide are commonly fabricated with metal materials, so that the distance between them is much smaller than the photon wavelength and even a channel is needed between them [56].

For the single-particle excitation, the state determined by Eq. (3) has the form

$$|\Psi\rangle = \int dx[\Phi_R(x,t)\hat{\psi}_R^\dagger(x) + \Phi_L(x,t)\hat{\psi}_L^\dagger(x)]|\varnothing\rangle + C(t)\hat{c}^\dagger|\varnothing\rangle + A(t)\hat{\sigma}_+|\varnothing\rangle, \tag{4}$$

where $|\varnothing\rangle$ is a vacuum state, implying that there is no photon whether in the waveguide or in the cavity, and that the ^{87}Rb atom is in the lower-energy state. $\Phi_{R/L}(x,t)$ are the wave functions of the right-/left-moving waveguide photons. $C(t)$ and $A(t)$, respectively, are the probability amplitudes of the cavity and atom. Substituting Eq. (4) into the Schrödinger equation of $i\partial_t|\Psi\rangle = \mathcal{H}|\Psi\rangle$, one can find the dynamical equations for $C(t)$, $A(t)$, $\Phi_R(x,t)$, and $\Phi_L(x,t)$ as follows:

$$i\partial_t C(t) = \tilde{\omega}_c C(t) + \frac{g}{2}A(t) + V_0[\Phi_R(0,t)+\Phi_L(0,t)], \tag{5a}$$

$$i\partial_t A(t) = \tilde{\omega}_a A(t) + \frac{g}{2}C(t), \tag{5b}$$

$$i\partial_t \Phi_R(x,t) = \hat{\omega}(-i\partial_x)\Phi_R(x,t) + V_0\delta(x)C(t), \tag{5c}$$

$$i\partial_t \Phi_L(x,t) = \hat{\omega}(+i\partial_x)\Phi_L(x,t) + V_0\delta(x)C(t). \tag{5d}$$

Since the waveguide dispersion is not linearized, these dynamical equations would be transformed into the reciprocal space for numerical calculation. With these equations, the dynamical properties of the system in Fig. 1(a) can be exactly analyzed. The right- and left-moving photon numbers, n_r and n_l, are given by

$$n_r = \int dx|\Phi_R(x,t)|^2, \quad n_l = \int dx|\Phi_l(x,t)|^2. \tag{6}$$

In calculation, a Gaussian-type pulse for the incident wave is adopted, namely,

$$\Phi_{\text{in}}(k) = \left(\frac{2}{\pi k_w^2}\right)^{\frac{1}{4}} e^{-(k-k_i)^2/k_w^2}, \tag{7}$$

where k is the wave vector with the pulse width of $2k_w^{-1}$. k_i represents the center wave vector, corresponding to the energy of $\varepsilon_i = c\sqrt{k_z^2 + k_i^2}$. For definiteness, we list the parameters used throughout the work here. The units of the frequency, time, length, and wave vector, respectively, are $\omega_0 = 2\pi \times 10^{10}$ Hz, $\tau_0 = 2\pi/\omega_0$, $\lambda_0 = 3$ cm, and $k_0 = 2\pi/\lambda_0$. Other parameters that remain unchanged in calculation are: $k_z = 2.245k_0$, $c = 3 \times 10^8$ m/s, $\omega_1 = 2.7\omega_0$, $\omega_2 = 0.7\omega_0$, and $\omega_c = \omega_1$. For the transition energy of the ^{87}Rb atom we consider two values, namely, $\omega_a = \omega_1$ or ω_2, which are used for the switch on and off states, respectively. The switch on and off states correspond to the fact that the couplings between the cavity and atom are "tuning" (i.e., $\omega_c = \omega_a = \omega_1$) and "detuning" (i.e., $\omega_c = \omega_1$, $\omega_a = \omega_2$). To quantify the switch, we introduce the on/off ratio as

$$\xi = \frac{T_{\text{Tun}}}{T_{\text{Detun}}}. \tag{8}$$

T_{Tun} and T_{Detun} are the transmissivities of the single photon pulse with the frequency $\varepsilon_i = \omega_1$ for the switch on and off states, respectively.

Since the nonlinear dispersion of $\omega(k)$ is adopted for the waveguide, we first transform the dynamical equation (5) into the reciprocal space and then numerically find the dynamical properties of the system. Initially, for the JC model the ^{87}Rb atom is in the lower-energy state and there is no photon in the cavity. For the waveguide the single microwave photon incident from the left side is described by Eq. (7). In the solving process the fourth-order Runge-Kutta and predictor-corrector methods are used in the reciprocal space discretized into the grid with 2^{11} points.

III. NUMERICAL RESULTS AND DISCUSSION

Figures 2(a)–2(c) show the transmission spectra of the single photon pulse for the tuning ($\omega_a = \omega_1$) and detuning ($\omega_a = \omega_2$) couplings between the cavity and atom. The transmission dips are mainly determined by the eigenvalues of $\mathcal{H}_{\text{JC}}$, namely,

$$\varepsilon_\pm = \tfrac{1}{2}[(\tilde{\omega}_c + \tilde{\omega}_a) \pm \sqrt{(\tilde{\omega}_c - \tilde{\omega}_a)^2 + g^2}]. \tag{9}$$

Since $\gamma_c = \gamma_a = 0$ is adopted in Fig. 2, we have $\tilde{\omega}_{c/a} = \omega_{c/a}$ and $\varepsilon_\pm = 2.7\omega_0 \pm 0.5g$ for the tuning coupling and $\varepsilon_\pm = 1.7\omega_0 \pm\sqrt{\omega_0^2 + g^2/4}$ for the detuning one. Between ε_+ and ε_- there is a transmission peak. For the tuning coupling it locates at ω_1, while ω_1 approaches the transmission dip position for the detuning coupling. These two situations can naturally be taken as the switch on and off states for the single photon with frequency ω_1. The corresponding wave vector $k_1 = 1.5k_0$ and wavelength $\lambda_1 = 2\lambda_0/3 = 2$ cm. Since the atom transition frequencies of ω_1 and ω_2 relate to the external electrostatic fields of 530 and 545.9 V/cm, the switch on and off states can be changed into each other conveniently. When $\gamma_c = \gamma_a = 0$, for the plane-wave input ($k_w \to 0$) the local minimum and maximum of the transmissivity around the transmission dips (switch off) and peaks (switch on) are strictly equal to zero and 1, respectively. However, these ideal cases would be broken by the finite width of the incident pulse, losses of the cavity and atom, or Rabi coupling. The incident pulse contains more plane-wave components as k_w increases, with the result that the transmission spectra become flatter, especially around the transmission dips and peaks [see Fig. 2(a)]. Correspondingly, the transmissivity decreases and increases for the switch on and off states as k_w increases [see the solid black and dashed

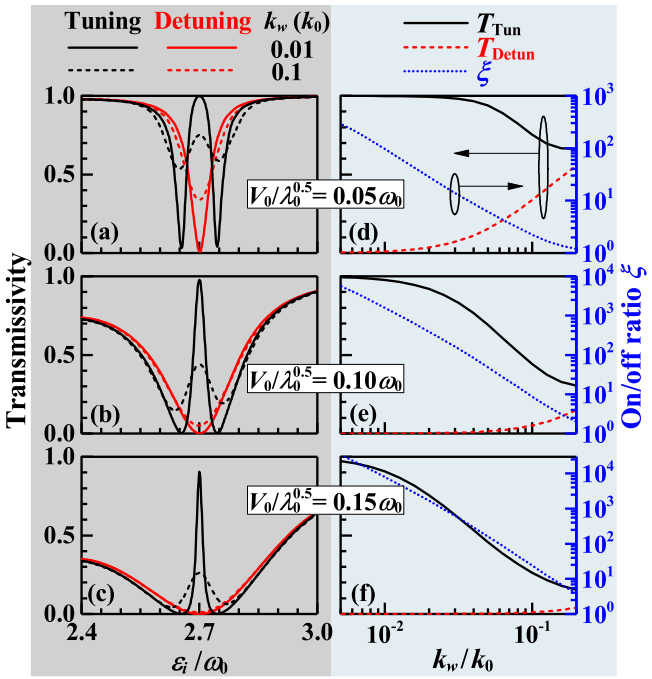

FIG. 2. (a–c) Transmission spectra of the single photon pulse with $k_w = 0.01k_0$ and $0.1k_0$ for the tuning and detuning couplings between the cavity and atom; (d–f) Variation of the transmissivity (solid black and dashed red curves, left axes) and on/off ratio (dotted blue curves, right axes) with k_w when $\varepsilon_i = 2.7\omega_0$. Parameters: $g = 0.09\omega_0$ and $\gamma_c = \gamma_a = 0$.

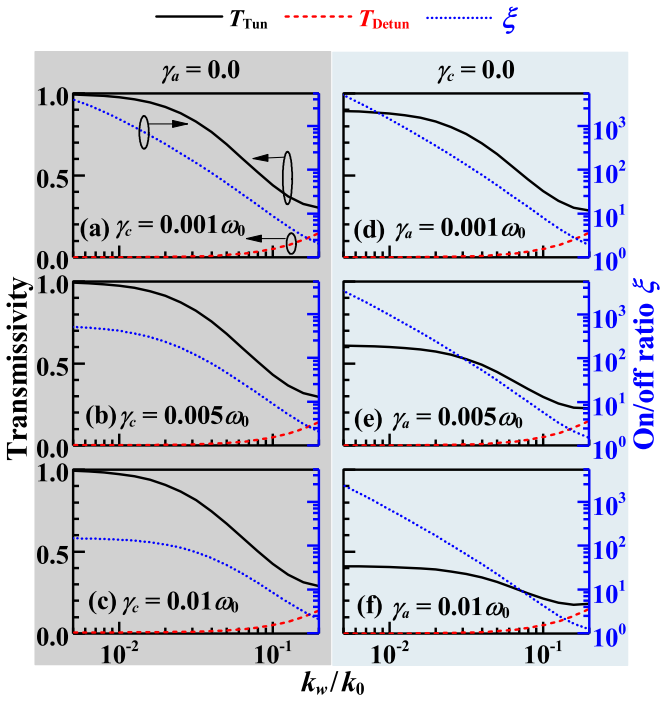

FIG. 3. Variation of the transmissivity (solid black and dashed red curves, left axes) and on/off ratio (dotted blue curves, right axes) with k_w under several different losses of the cavity and atom. Parameters: $g = 0.09\omega_0$, $V_0/\lambda_0^{0.5} = 0.1\omega_0$, and $\varepsilon_i = 2.7\omega_0$.

red curves in Fig. 2(d)]. As a result, the on/off ratio ξ [see the dotted blue curve in Fig. 2(d)] decreases from 2.9×10^2 to 2.2 when k_w increases from $0.005k_0$ to $0.1k_0$, implying that the switch cannot work well for the ultranarrow pulse. This nodus can partially be overcome by increasing the coupling between the waveguide and cavity. For example, $\xi \approx 8.7$ and 2.4×10^1, respectively, when $V_0/\lambda_0^{0.5} = 0.1\omega_0$ and $0.15\omega_0$ for $k_w = 0.1k_0$ [see Figs. 2(e) and 2(f)]. If $\xi > 10^2$ is required for a switch, Fig. 2(f) shows that k_w should be smaller than $0.06k_0$, that is, the pulse width should be larger than 15.9 cm, being about 8 times that of the photon wavelength λ_1. Moreover, the on/off ratio can reach a much larger value for a broad pulse. For example, when $k_w = 0.005k_0$ the on/off ratio is up to 5.6×10^3 and 3.4×10^4 for $V_0/\lambda_0^{0.5} = 0.1\omega_0$ and $0.15\omega_0$, respectively [refer to Figs. 2(e) and 2(f)].

The on/off ratio also depends on the losses of the cavity and atom, as shown in Fig. 3 where $V_0/\lambda_0^{0.5} = 0.1\omega_0$. Figures 3(a)–3(c) show that ξ decreases as γ_c increases. In addition, ξ has a saturation behavior for large γ_c [see Figs. 3(b) and 3(c)]. This can be understood by the transmission coefficient of the plane wave ($k_w \to 0$) with the energy ε_i [55],

$$t = \frac{1}{1 + i\frac{V_0^2/v_g}{\varepsilon_i - \omega_c + i\gamma_c - \frac{g^2/4}{\varepsilon_i - \omega_a + i\gamma_a}}}, \tag{10}$$

where the group velocity $v_g = \frac{d\omega(k)}{dk}|_{\omega(k)=\omega_1} \approx 0.56c$. To obtain Eq. (10) the dispersion of the waveguide mode has been linearized near the cavity energy ω_c, namely, $\omega(k) = \omega_c + v_g(k - k_1)$. For the tuning coupling $T_{\rm Tun} = |\frac{\gamma_a\gamma_c + g^2/4}{\gamma_a(\gamma_c + V_0^2/v_g) + g^2/4}|^2$, where $\varepsilon_i = \omega_c = \omega_a = 2.7\omega_0$, while for the detuning coupling $T_{\rm Detun} = |\frac{\gamma_a\gamma_c + g^2/4 - i2\omega_0\gamma_c}{\gamma_a(\gamma_c + V_0^2/v_g) + g^2/4 - i2\omega_0(\gamma_c + V_0^2/v_g)}|^2$, where $\varepsilon_i = \omega_c = 2.7\omega_0$ and $\omega_a = 0.7\omega_0$. Note that these two expressions are valid only for the plane-wave incidence, giving the saturation value of ξ as $k_w \to 0$:

$$\xi_{\rm sat} = \left[\frac{\gamma_a\gamma_c + g^2/4}{\gamma_a(\gamma_c + V_0^2/v_g) + g^2/4}\right]^2 \times \frac{\left[\gamma_a(\gamma_c + V_0^2/v_g) + g^2/4\right]^2 + 4\omega_0^2(\gamma_c + V_0^2/v_g)^2}{(\gamma_a\gamma_c + g^2/4)^2 + 4\omega_0^2\gamma_c^2}. \tag{11}$$

From $\xi_{\rm sat}$ one can see that γ_a and γ_c strongly influence the on/off ratio. For $\gamma_a = 0$, $\xi_{\rm sat} = \frac{(g^2/4)^2 + 4\omega_0^2(\gamma_c + V_0^2/v_g)^2}{(g^2/4)^2 + 4\omega_0^2\gamma_c^2} \sim 6.4 \times 10^3$, 5.3×10^2, and 1.5×10^2 when $\gamma_c = 0.001\omega_0$, $0.005\omega_0$, and $0.01\omega_0$, respectively. They are the limitation of the on/off ratios shown in Figs. 3(a)–3(c). For $\gamma_c = 0$, we can find $\xi_{\rm sat} = 1 + |\frac{2\omega_0}{\gamma_a + g^2/(4V_0^2/v_g)}|^2$. Because $g^2/(4V_0^2/v_g)$ ($\sim 0.02\omega_0$) is larger than γ_a used in Figs. 3(d)–3(f), the decrease of ξ is slower for increasing γ_a than increasing γ_c. The corresponding saturation values are 1.1×10^4, 7.5×10^3, and 5.1×10^3 for Figs. 3(d)–3(f), much larger than those in Figs. 3(a)–3(c), respectively. Therefore, a high-Q cavity is required. Considering that ξ is larger than 100 for the pulse width $k_w < 0.02k_0$ when $Q \sim \frac{\omega_1}{\gamma_c} = 270$, refer to Fig. 3(c), it is possible in practice to design such a single microwave photon switch. In addition, the

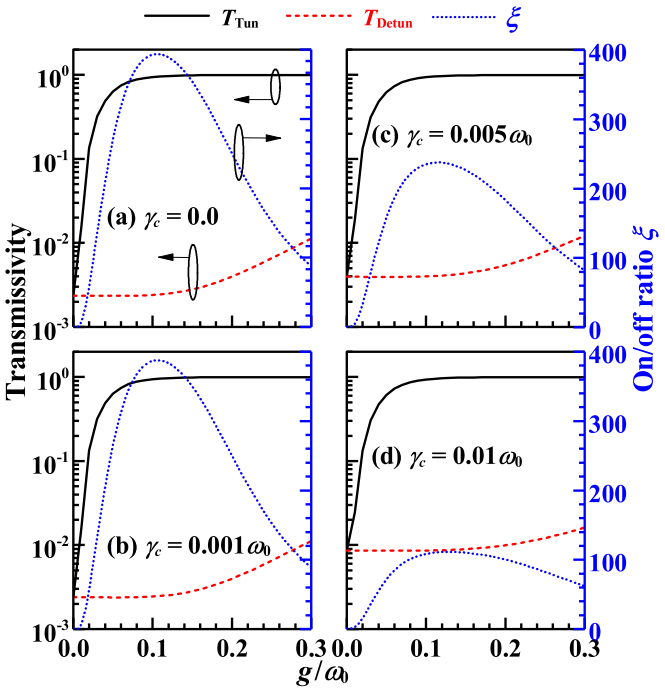

FIG. 4. Variation of the transmissivity (solid black and dashed red curves, left longitudinal axes) and on/off ratio (dotted blue curves, right axes) with g under several losses of the cavity. Parameters: $V_0/\lambda_0^{0.5} = 0.1\omega_0$, $\varepsilon_i = 2.7\omega_0$, $k_w = 0.02k_0$, and $\gamma_a = 0$.

above discussions also show that the on/off ratio can be up to 1000 in certain cases.

As shown in Eq. (9) the energy levels of the JC model depend on the Rabi coupling between the cavity and atom, and so do the transmissivities $T_{\rm Tun}$ and $T_{\rm Detun}$ (refer to Fig. 4), where $\gamma_a = 0$ is adopted for it shows weaker influence on ξ than γ_c. The transmission peak for the tuning coupling is always located at the energy of ω_1 no matter what the value of g is, while the position of the transmission dip for the detuning coupling gradually walks away from ω_1 as g increases. Consequently, $T_{\rm Tun}$ and $T_{\rm Detun}$ both increase for increasing g, with the result that ξ first increases and then decreases. This can be argued as follows. For small g the two transmission dips are too close to each other for the tuning coupling, leading to small $T_{\rm Tun}$. On the contrary, for large g the position of the transmission dip is far away from ω_1 for the detuning coupling, leading to large $T_{\rm Detun}$. Both situations result in small ξ, implying that there is a best choice for g (see Fig. 4). One can derive the best choice by setting the derivative of $\xi_{\rm sat}$ in Eq. (11) with respect to g to be zero, but the expression is too complicated to find a concise result. Numerical calculation in Figs. 4(a)–4(d) shows that such a value of g depends on γ_a and γ_c obviously but not strongly. The best choice is about several percent of the incident photon energy (i.e., $\varepsilon_i = 2.7\omega_0$) and is in the range of $(0.08,\ 0.16)\omega_0$, which benefits the design of the switch.

In order to confirm the feasibility of the switch, we plot the time evolution of the waveguide photon probability densities in Figs. 5(a) and 5(c), where the switch state is changed from on to off and from off to on, respectively, during the scattering process. The change of the switch state results in

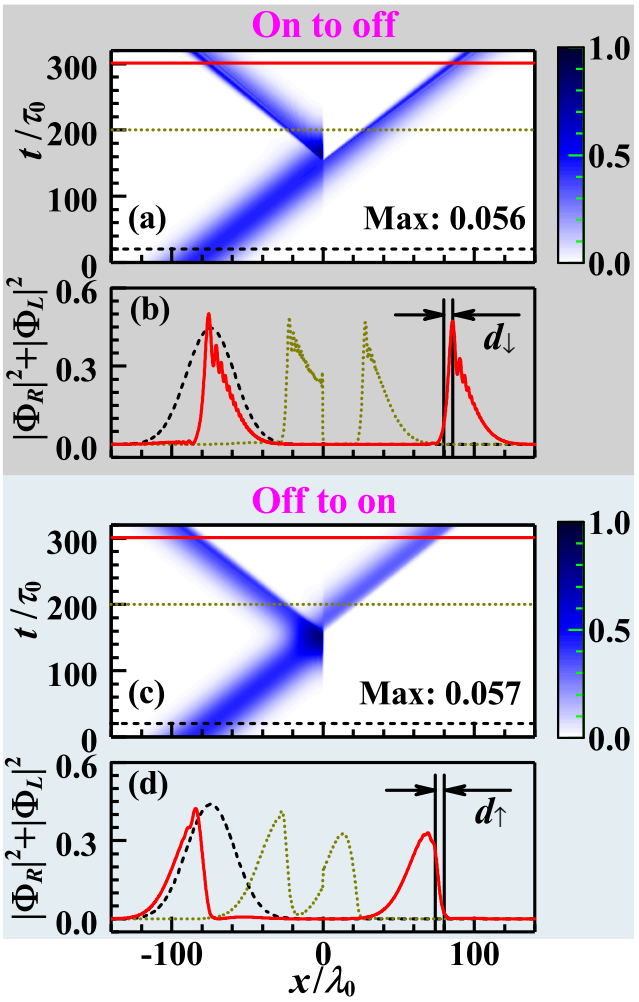

FIG. 5. (a) Contour map of the waveguide photon probability density (normalized to its maximum value denoted by "Max") as functions of x and t for the switch first turning on and then off and (b) the probability distributions when $t = 20\tau_0$ (dashed black), $200\tau_0$ (dotted dark yellow), and $300\tau_0$ (solid red), corresponding to those in (a). The denotations for (c) and (d) are the same as those for (a) and (b), except the switch first turning off and then on. Parameters: $V_0/\lambda_0^{0.5} = 0.1\omega_0$, $g = 0.09\omega_0$, k_w=0.01k_0, $\gamma_c = 0.005\omega_0$, and $\gamma_a = 0$.

a sharp variation for the transmitted and reflected probability densities, which compensates with each other under a vertical mirror symmetry operation along the line of $x = 0$. In other words, the transmitted and reflected pulses are tailored into non-Gaussian waveforms, being quite different from that of the incident pulse. For analyzing the time response of the switch we introduce $\tau_\downarrow$ ($\tau_\uparrow$) to measure the decay (rise) time for the transmitted probability decreasing from 1 to $\frac{1}{e}$ (increasing from $\frac{1}{e}$ to 1) times that of its maximum. This can be read from Figs. 5(b) and 5(d), where the probability densities in Figs. 5(a) and 5(c) at the time of $20\tau_0$, $200\tau_0$, and $300\tau_0$ are plotted. The probability densities at the time of $20\tau_0$ give the incident Gaussian pulse, while those at the time of $200\tau_0$ and $300\tau_0$ tell the transmitted ($x > 0$) and reflected ($x < 0$) pulses near and after the scattering process. When the switch is turned

off the transmission is hindered; see the left and right sides of the transmitted pulses in Figs. 5(b) and 5(d).

The decay (rise) time is reflected by the decay (rise) distance of the probability density in the real space; see $d_\downarrow$ ($d_\uparrow$) in Fig. 5(b) [Fig. 5(d)]. They connect with each other by

$$\tau_\downarrow = \frac{d_\downarrow}{v_g}, \quad \tau_\uparrow = \frac{d_\uparrow}{v_g}, \tag{12}$$

where $v_g \approx 0.56c$. From Figs. 5(b) and 5(d) one can estimate $d_\downarrow \approx 3.9\lambda_0$ and $d_\uparrow \approx 4.2\lambda_0$ and therefore, $\tau_\downarrow \approx 7.0\tau_0$ and $\tau_\uparrow \approx 7.5\tau_0$, indicating that the switch can work well only when the width of the incident pulse is larger than $v_g(\tau_\uparrow + \tau_\downarrow) \approx 8.1\lambda_0$. Under this condition the on/off ratio can be up to 100 as $\gamma_c < 0.005\omega_0$ [see Fig. 3(b)]. In terms of k_w, the condition is changed such that k_w should be less than $0.04k_0$, which is met by k_w used for the incident pulse in Fig. 5. In addition, Fig. 2 has shown that the narrower the pulse width is, the less the on/off ratio becomes. These two limitations both prefer small k_w. Combining all above numerical results, we find that the on/off ratio can be up to or even larger than 100, simultaneously with the decay time and rise time being both about $7.5\tau_0 = 0.75$ ns when $k_w < 0.04k_0$, $V_0/\lambda_0^{0.5} \gtrsim 0.1\omega_0$, and $g \in (0.08\ , 0.16)\omega_0$. The switch operating frequency is determined by the Rydberg atom, being $2\pi \times 27$ GHz in this work.

Though the non-Hermitian Hamiltonian in Eq. (3) has shown that the designed switch is practical in experiments, the system quantum noise may degrade its performance, especially the on/off ratio. To show this we introduce the density matrix $\hat{\rho}$ and the Lindblad master equation [57], written as

$$i\frac{\partial}{\partial t}\hat{\rho} = [\mathcal{H},\ \hat{\rho}] + iD\hat{\rho}, \tag{13}$$

where

$$D\hat{\rho} = \gamma_c([\hat{c}\hat{\rho},\ \hat{c}^\dagger] + [\hat{c},\ \hat{\rho}\hat{c}^\dagger]) + \gamma_a([\hat{\sigma}_-\hat{\rho},\ \hat{\sigma}_+] + [\hat{\sigma}_-,\ \hat{\rho}\hat{\sigma}_+]). \tag{14}$$

After expressing Eq. (13) in single-particle space we can find the time evolution of $\hat{\rho}$. The losses of γ_c and γ_a are due to the influence of the quantum noise on the JC system. A numerical scheme similar to that for Eq. (5) is adopted. Figure 6 (whose parameters are the same with those in Fig. 5) shows the time evolutions of the probability density and particle number for the waveguide photon. The incident waveguide photon can transport through the JC system as the switch is on [see Figs. 6(a) and 6(b)], while it is reflected as the switch is off [see Figs. 6(c) and 6(d)]. Their transmissivities respectively are $T_{\text{Tun}} = 0.975$ and $T_{\text{Detun}} = 0.061$, giving the on/off ratio $\xi = 16.0$. Since this value is smaller than that obtained from Eq. (5) [refer to Fig. 3(b)], the quantum noise can reduce the switch ratio. Because the on/off ratio is still large enough, the designed switch is practical for application.

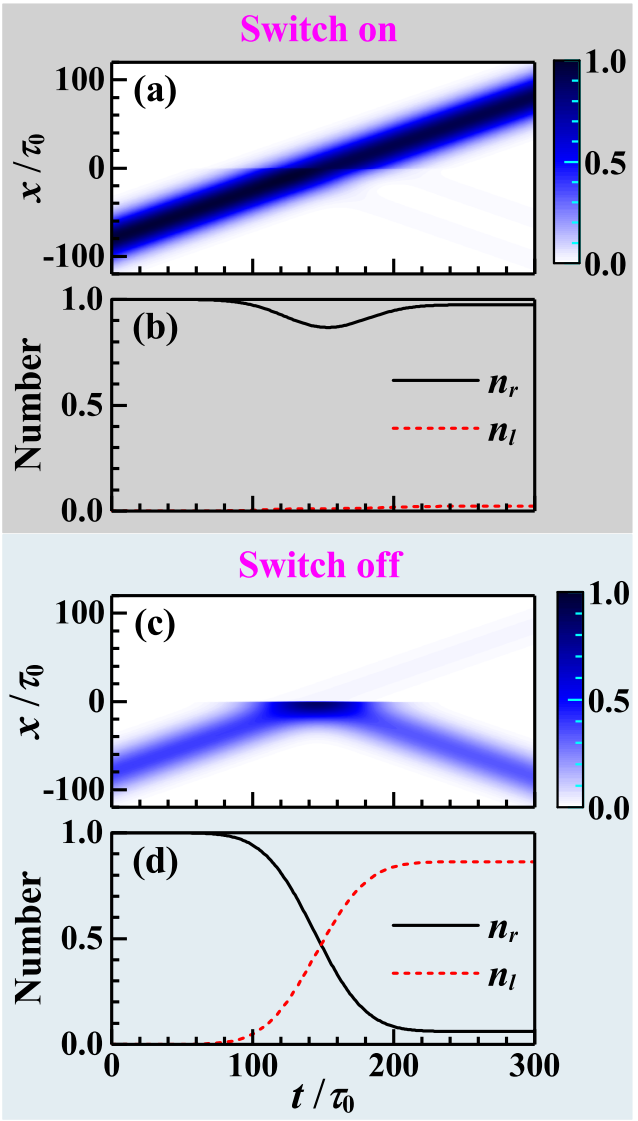

FIG. 6. (a) Contour map of the waveguide photon probability density (normalized to its maximum value) as functions of x and t for the switch on state and (b) corresponding time evolution of n_r and n_l. (c) and (d) are the same as (a) and (b), respectively, except for the switch off state. Parameters: $V_0/\lambda_0^{0.5} = 0.1\omega_0$, $\varepsilon_i = 2.7\omega_0$, $g = 0.09\omega_0$, k_w=$0.01k_0$, $\gamma_c = 0.005\omega_0$, and $\gamma_a = 0$.

IV. CONCLUSION

In this work, we designed a single microwave photon switch based on a one-dimensional waveguide. The quantum emitter of a single-mode cavity with an embedded Rydberg atom ^{87}Rb is used to control the transmission of the single photon pulse. Since the energy spectra of the ^{87}Rb atom can be controlled by an external electrostatic field, therefore the ^{87}Rb atom could be in resonance or out of resonance with the cavity by adjusting the external electrostatic field. These two situations give the switch on and off states, respectively. Because the single photon pulse contains many plane-wave components, the on/off ratio decreases for increasing the pulse width, which can be overcome by increasing the coupling between the waveguide and cavity. For the Rabi coupling there is a best choice, being about several percent of the incident photon energy. Moreover, the atom dissipation shows a weaker influence on the on/off ratio with respect to the cavity dissipation. For the widely used values of the model parameters the on/off ratio can be larger than 100, and simultaneously the decay time and rise time are both about 0.75 ns. The transition energy of the two-level Rydberg atom gives the switch operating frequency, being $2\pi \times 27$ GHz in this work.

At last, the master equation of the density matrix was used to demonstrate that the on/off ratio can be reduced by the quantum noise but is still large enough for application. Therefore, the designed single photon switch is viable in practice and has potential in quantum informatics.

ACKNOWLEDGMENTS

This work is supported by the NSFC (Grant No. 11304015) and the Beijing Higher Education Young Elite Teacher Project (Grant No. YETP1228).

[1] D. Englund, A. Majumdar, A. Faraon, M. Toishi, N. Stoltz, P. Petroff, and J. Vučković, Phys. Rev. Lett. **104**, 073904 (2010).
[2] M. T. Cheng and Y. Y. Song, Opt. Lett. **37**, 978 (2012).
[3] J. F. Huang, T. Shi, C. P. Sun, and F. Nori, Phys. Rev. A **88**, 013836 (2013).
[4] J. Q. Liao and C. K. Law, Phys. Rev. A **87**, 043809 (2013).
[5] J. T. Shen and S. Fan, Phys. Rev. Lett. **98**, 153003 (2007).
[6] S. Fan, Ş. E. Kocabaş, and J. T. Shen, Phys. Rev. A **82**, 063821 (2010).
[7] E. Rephaeli, Ş. E. Kocabaş, and S. Fan, Phys. Rev. A **84**, 063832 (2011).
[8] D. Roy, Phys. Rev. Lett. **106**, 053601 (2011).
[9] P. Longo, P. Schmitteckert, and K. Busch, Phys. Rev. A **83**, 063828 (2011).
[10] H. Zheng, D. J. Gauthier, and H. U. Baranger, Phys. Rev. A **85**, 043832 (2012).
[11] D. Roy, Phys. Rev. A **87**, 063819 (2013).
[12] T. Shi, S. Fan, and C. P. Sun, Phys. Rev. A **84**, 063803 (2011).
[13] Z. Ji and S. Gao, Opt. Commun. **285**, 1302 (2012).
[14] J. Q. Liao and C. K. Law, Phys. Rev. A **82**, 053836 (2010).
[15] M. Tokushima, H. Kosaka, A. Tomita, and H. Yamada, Appl. Phys. Lett. **76**, 952 (2000).
[16] M. Notomi, K. Yamada, A. Shinya, J. Takahashi, C. Takahashi, and I. Yokohama, Phys. Rev. Lett. **87**, 253902 (2001).
[17] S. Lan, K. Kanamoto, T. Yang, S. Nishikawa, Y. Sugimoto, N. Ikeda, H. Nakamura, K. Asakawa, and H. Ishikawa, Phys. Rev. B **67**, 115208 (2003).
[18] E. Kuramochi, M. Notomi, S. Hughes, A. Shinya, T. Watanabe, and L. Ramunno, Phys. Rev. B **72**, 161318 (2005).
[19] G. Brambilla, F. Xu, P. Horak, Y. Jung, F. Koizumi, N. P. Sessions, E. Koukharenko, X. Feng, G. S. Murugan, J. S. Wilkinson, and D. J. Richardson, Adv. Opt. Photon. **1**, 107 (2009).
[20] G. Brambilla, J. Opt. **12**, 043001 (2010).
[21] A. Manekkathodi, Y. J. Wu, L. W. Chu, S. Gwo, L. J. Chou, and L. J. Chen, Nanoscale **5**, 12185 (2013).
[22] R. D. Kekatpure, E. S. Barnard, W. Cai, and M. L. Brongersma, Phys. Rev. Lett. **104**, 243902 (2010).
[23] Y. Huang, C. Min, and G. Veronis, Appl. Phys. Lett. **99**, 143117 (2011).
[24] Z. Han and S. I. Bozhevolnyi, Opt. Express **19**, 3251 (2011).
[25] J. Chen, C. Wang, R. Zhang, and J. Xiao, Opt. Lett. **37**, 5133 (2012).
[26] Y. F. Xiao, M. Li, Y. C. Liu, Y. Li, X. Sun, and Q. Gong, Phys. Rev. A **82**, 065804 (2010).
[27] X. Tu, L. Y. Mario, and T. Mei, Opt. Express **18**, 18820 (2010).
[28] H. Lu, X. Liu, D. Mao, and G. Wang, Opt. Lett. **37**, 3780 (2012).
[29] D. O'Shea, C. Junge, J. Volz, and A. Rauschenbeutel, Phys. Rev. Lett. **111**, 193601 (2013).
[30] G. Dong, Y. Zhang, M. A. Kamran, and B. Zou, J. Appl. Phys. **113**, 143105 (2013).
[31] M. Gullans, D. E. Chang, F. H. L. Koppens, F. J. García de Abajo, and M. D. Lukin, Phys. Rev. Lett. **111**, 247401 (2013).
[32] T. Shi and S. Fan, Phys. Rev. A **87**, 063818 (2013).
[33] S. Xu, E. Rephaeli, and S. Fan, Phys. Rev. Lett. **111**, 223602 (2013).
[34] S. Fan, Appl. Phys. Lett. **80**, 908 (2002).
[35] S. Sandhu, M. L. Povinelli, and S. Fan, Appl. Phys. Lett. **96**, 231108 (2010).
[36] L. Neumeier, M. Leib, and M. J. Hartmann, Phys. Rev. Lett. **111**, 063601 (2013).
[37] J. Pan, Y. Huo, S. Sandhu, N. Stuhrmann, M. L. Povinelli, J. S. Harris, M. Fejer, and S. Fan, Appl. Phys. Lett. **97**, 101102 (2010).
[38] G. Dong, Y. Zhang, J. F. Donegan, B. Zou, and Y. Song, Plasmonics **9**, 1085 (2014).
[39] K. C. Fan, W. L. Lin, L. H. Chiang, S. H. Chen, T. T. Chung, and Y. J. Yang, J. Lightwave Technol. **27**, 1155 (2009).
[40] A. Sharkawy, S. Shi, D. W. Prather, and R. A. Soref, Opt. Express **10**, 1048 (2002).
[41] C. Nuckolls, R. Shao, W. G. Jang, N. A. Clark, D. M. Walba, and T. J. Katz, Chem. Mater. **14**, 773 (2002).
[42] M. Scalora, J. P. Dowling, C. M. Bowden, and M. J. Bloemer, Phys. Rev. Lett. **73**, 1368 (1994).
[43] C. Min, P. Wang, C. Chen, Y. Deng, Y. Lu, H. Ming, T. Ning, Y. Zhou, and G. Yang, Opt. Lett. **33**, 869 (2008).
[44] D. Yu, A. Landra, M. M. Valado, C. Hufnagel, L. C. Kwek, L. Amico, and R. Dumke, Phys. Rev. A **94**, 062301 (2016).
[45] J. M. Raimond, M. Brune, and S. Haroche, Rev. Mod. Phys. **73**, 565 (2001).
[46] A. A. Houck, D. I. Schuster, J. M. Gambetta, J. A. Schreier, B. R. Johnson, J. M. Chow, L. Frunzio, J. Majer, M. H. Devoret, S. M. Girvin, and R. J. Schoelkopf, Nature (London) **449**, 328 (2007).
[47] Z. H. Peng, S. E. de Graaf, J. S. Tsai, and O. V. Astafiev, Nat. Commun. **7**, 12588 (2016).
[48] J. Lindkvist and G. Johansson, New J. Phys. **16**, 055018 (2014).
[49] A. Carmele, B. Vogell, K. Stannigel, and P. Zoller, New J. Phys. **16**, 063042 (2014).
[50] T. Tanabe, M. Notomi, S. Mitsugi, A. Shinya, and E. Kuramochi, Appl. Phys. Lett. **87**, 151112 (2005).
[51] D. M. Beggs, T. P. White, L. O'Faolain, and T. F. Krauss, Opt. Lett. **33**, 147 (2008).
[52] X. Wei, J. Zhang, and Y. Zhu, Phys. Rev. A **82**, 033808 (2010).
[53] M. L. Zimmerman, M. G. Littman, M. M. Kash, and D. Kleppner, Phys. Rev. A **20**, 2251 (1979).
[54] M. Marinescu, H. R. Sadeghpour, and A. Dalgarno, Phys. Rev. A **49**, 982 (1994).
[55] Y. Zhang and B. Zou, Phys. Rev. A **89**, 063815 (2014).
[56] P. A. George, C. Manolatou, F. Rana, A. L. Bingham, and D. R. Grischkowsky, Appl. Phys. Lett. **91**, 191122 (2007).
[57] H.-P. Breuer and F. Petruccione, *The Theory of Open Quantum Systems* (Oxford University Press, Oxford, UK, 2007).